ARTICLE

Effective replacement of cetyltrimethylammonium bromide (CTAB) by mercaptoalkanoic acids in the gold nanorods (AuNRs) surfaces in aqueous solutions

Received 00th January 20xx,
Accepted 00th January 20xx

DOI: 10.1039/x0xx00000x

Rafael del Caño,[a] Jose M. Gisbert-González,[a] Jose González-Rodríguez,[b] Guadalupe Sánchez-Obrero,[a] Rafael Madueño,[a] Manuel Blázquez,[a] Teresa Pineda[a*]

The highly packed cetyltrimethylammonium bromide (CTAB) bilayer built up on the surface of gold nanorods (AuNRs) when synthetized by the seed-mediated procedure hampers the complete ligand exchange under experimental conditions that preserve the stability of the dispersions. In the present work, a ligand exchange protocol by using carboxy-terminated alkanethiols of different chain length by means of a green approach that use only aqueous solutions is presented. The protocol is based on the kwnoledge of the stability in aqueous solution of both, the starting CTAB-AuNRs and the final products that help in the choice of the experimental conditions used for ligand exchange. The characterization of the CTAB protective layer as well as the study of its colloidal estability in solution have helped us to design the appropriate methodology. Cyclic voltammetry of CTAB-AuNRs demonstrates the high stability of the bilayer showing the existence of a two-dimensional phase transition from a highly ordered to a less organized phase. Other techniques such as XPS, FT-IR and Raman spectroscopies inform about the structure of the layer and UV-visible-NIR spectroscopy stablishes the stability conditions in aqueous solution. We have chosen an exchange procedure for 11-mercaptoundecanoic acid (MUA) and 16-mercaptohexadecanoic acid (MHDA) based in a one-pot methodology under conditions where all the species involved are stable. The protocol, however, can be extended to different chemical functionalities that are considered useful to be applied in living systems. Under these conditions the complete exchange of CTAB by the mercaptoderivatives was successful as demonstrated by the different characterization techniques used: UV-visible-NIR, FT-IR, Raman, XPS spectroscopy, cyclic voltammetry and transmission electron microscopy (TEM).

1. Introduction

The high sensitivity to the refraction index of the surrounding media derived from the anisotropic shape of nanomaterials confers a great potential for biological applications.[1] Although gold nanorods (AuNRs) are the most studied anisotropic nanomaterials, its use in living systems is restricted due to the known toxicity of cetyltrimethylammonium bromide (CTAB) molecules that come from the seed mediated synthesis procedure that utilizes large concentrations of this surfactant that forms a tightly bound bilayer on the AuNR surface.[2, 3] The very well documented toxicity as well as its ability of insertion on the cellular membranes [4] recommend their elimination from the surface to make the AuNRs useful in biological systems. The synthesis procedure employs high CTAB concentrations (~ 0.1 M) but if both, the surface area of the AuNRs contained in a preparation and the typical packing density are considered, the CTAB bound molecules necessary for AuNRs colloidal stability needs to be on the micromolar order. However, AuNRs become unstable when transferred to low surfactant concentration solutions (~0.1 mM < CTAB < 1 mM, in the order of its critical micelle concentration) and the continuous exchange between the free, bound and micellar CTAB led to the deprotection against aggregation.[5, 6]

The existence of a bilayer around the pristine AuNR is widely accepted and has been demonstrated by different characterization techniques such as IR spectroscopy, thermogravimetric analysis and zeta potential measurements.[7-9] Moreover, the appearance of a Raman signal due to the Br-Au bond suggests that the hydrophobic alkane chain would be exposed to the solution while the trimethyl ammonium head would interact with the bromide adsorbed in the surface.[10] This organization facilitates the formation of the second layer. The role of the bromide have been determined adding trace amount of iodide anions that provoke the formation of nanoparticles of different shapes.[11-13]

The pioneering works describing the seed-mediated protocols by Murphy and El-Sayed teams [14-16] used CTAB and

[a] Department of Physical Chemistry and Applied Thermodynamics, Institute of Fine Chemistry and Nanochemistry, University of Cordoba, Campus Rabanales, Ed. Marie Curie 2ª Planta, E-14014 Córdoba, Spain.
[b] School of Chemistry, College of Science, University of Lincoln, Brayford Pool, Lincoln LN67TS, UK Address here.
† Footnotes relating to the title and/or authors should appear here.
Electronic Supplementary Information (ESI) available: [details of any supplementary information available should be included here]. See DOI: 10.1039/x0xx00000x

other chemicals to direct the growth of the anisotropic crystals. Although there have been many attempts to avoid the use of CTAB [17] these methods are not reproducible and the homogeneity of the samples obtained is not good. The role of the surfactant in the formation of the nanorod has been studied by molecular dynamics simulations [18] and it has been found that the anisotropic growth is facilitated by the epitaxial adsorption of CTAB in the developed facets. This is a consequence of the different adsorption energies that induce passivation at the (110) and (100) facets and mediate the crystal growth through a preferential reduction in the (111) facet. Moreover, it is very important to highlight the role of the micellar morphology and the surface chemistry [1, 16, 19-21] in the ability of CTAB to effectively passivate the epitaxial gold surfaces that, at the end, is dictated by the ionic strength and the counterions population.[15]

The role of the Ag^+ ions employed in the seed mediated procedures to improve the homogeneity and yield of nanorods has also been addressed.[16] Crystallographic analyses show that Ag^+ ions induce the formation of single crystals in which the longitudinal growth is in the <001> direction and the tip is formed by (110) and (111) facets, while the rod consists of eight facets of the (250) higher index.[22] It has been proposed that the Ag^+ ions have a direct effect in the CTA^+ adsorption. Fine structure X-ray studies indicate that Ag is present on the nanorod surface [23] and that it is adsorbed through an underpotential deposition process [24] probably taking place at the (110) longitudinal facets, passivating them and provoking an anisotropic growth that creates a surface for improved CTAB adsorption. A complex of the type CTA^+AgBr^{2-} has been proposed as the active surfactant on the basis of XPS measurements [25] and is supposed to be responsible for the epitaxial adsorption changing the micellization of CTAB. However, structural characterization of the morphological evolution reveals that Ag directs the anisotropic facet growth rates at the early stages but as the reaction progresses, incorporates into the bulk of the nanorod.[26]

All this body of evidence allows to conclude that the role of CTAB is more complex than that of a surfactant passivating the surface. Moreover, the energetic considerations point to a strong interaction with gold with important implications. Therefore, the elimination of CTAB from the nanorod surface, through exchange reactions is not a mere exercise of molecule displacement as it happens with citrate-anions-covered nanoparticles.[27] The most used method for CTAB elimination from the AuNR surface consists on the washing of the suspensions to lower the concentration to a value just above the concentration that produce the AuNR aggregation. [15, 16, 28] Other suggested methods are based on the decrease of the residual CTAB by extraction from an ionic liquid immiscible phase that contains the hydrophobic thiolated ligands binding strongly to the gold surface by displacing the CTAB molecules, or by using organic solvents.[29, 30] Finally, it is possible to find in the literature methods using the replacement of CTAB with citrate anions or with a detergent during the washing process [19] or by using sodium borohydride followed by ligand replacement.[31]

The strategy of using thiolate ligands is preferred over the layer-by-layer approach that assembles zwitter-ionic molecules,[32] as the former allows for the complete elimination of CTAB. However, the ligand exchange approach is difficult and presents the risk of irreversible aggregation during the process due to an excessive destabilization of the CTAB bilayer before the passivation of the nanorod surface by the new ligand takes place. However, many protocols indicate that some CTAB molecules are trapped inside the new formed layer, especially when polymers as poly-ethylene glycol are used.[33]

Recent developments on the estate-of-the-art in this area have been made by considering the conditions to reach the complete ligand exchange. Thus, the incoming molecules are able to displace the CTAB from the nanorod surface, bind to and keep bound under different experimental conditions. The recent literature has focused in the development of strategies to use mercapto-derivatives, dithiocarbamates and cyclic disulfides that allow the binding of these molecules to the gold surface.[33] The strength of the semi-covalent S-Au bond (~45kcal/mol) increases the binding strength of the grafted molecule.[34] Moreover, the chemistry of thiols is very attractive and has led to a fast increase in the number of available molecules that bear a thiol group for ligand exchange. The most used approaches for ligand exchanges are the one-pot, phase-transfer and solid phase methods.[27, 33, 35-37] The one-pot method is the most direct way and is very well described for AuNPs modification.[27, 38-40] In this approach, the ligands are directly added to an aqueous solution by taking into account that the resultant products must keep solubility and stability under the experimental conditions.

In this work, we present a study of the synthesis of AuNRs and its surface modification by 11-mercaptoundecanoic acid (MUA) and 16-mercaptohexanoic acid (MHDA), molecules. The protocol used is based on a green approach that avoid the use of organic solvents and takes advantage of some reported results that establish the different conformations of the CTAB molecules in the bilayer, depending on the CTAB solution concentration.[6] As it has been pointed out in that report, the structural transition in the bilayer influences the displacement of the surfactant by thiolate derivatives. Thus, the choice of experimental conditions that allow the stability of both, the CTAB- and the derivatized-AuNRs, constitutes the basis for a simple methodology that eliminates the surfactant from the AuNR surface simultaneously with its modification with the desired thiol derivative by using a one-pot protocol that emphasizes in the preservation of the AuNRs stability during the ligand exchange procedure. A throughout characterization of the different specimens is reported based on experimental techniques such as UV-visible-NIR, FT-IR, Raman, XPS spectroscopies, electrochemical (cyclic voltammetry) and microscopy (TEM). These techniques inform on the structural properties and the identity of the molecules that protect and functionalize the AuNRs and are used with the aim of evidence the substitution of CTAB by the two assayed molecules. Moreover, this methodology is totally transferable to the use of other thiol derivatives by only taking care of the final stability conditions of the functionalized AuNRs that would depend on the chemistry of the exchanged ligands.

2. Results and discussion

We have prepared CTAB-AuNRs of two different sizes and low dispersity that show UV-visible spectra with bands at either 517 and 645 nm or 510 and 760 nm (Figure 1). The position of these bands indicates that the AuNRs have an average aspect ratio (AR) of 3 and 4, respectively.[16] However, when the AuNRs were examined by TEM, the average AR are 2.4 (length: 68±11, width: 30±6) and 3.8 (length: 63±12, width: 18±6 nm), respectively (Figure S1, Supporting information).

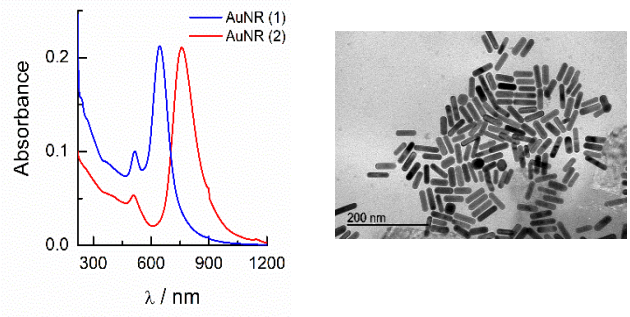

Figure 1. (left) UV-visible-NIR spectra of CTAB-AuNRs of different aspect ratio: (1) AR = 3, (2) AR = 4; (right) TEM images of the CTAB-AuNRs.

As stated above, the CTAB molecules form a very well packed bilayer on the nanorod surface where the CTA^+ first layer is seated on a bromide anions monolayer strongly bound to the gold surface. The trimethylammonium polar head is thus interacting with the bromide layer and the nonpolar terminal portion of the surfactant exposes to the solution and induces the formation of the bilayer. This is directed in the aqueous solution by the hydrophobic interactions as illustrated in Scheme 1.

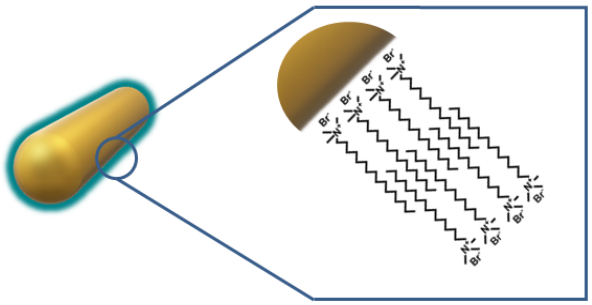

Scheme 1. Details of the CTAB-bilayer on the AuNRs surface.

Cyclic voltammetry characterization.

To get more information about the state of the CTAB bilayer, an aliquot of the CTAB-AuNRs suspension is drop-casted on a glassy carbon surface, dried with a nitrogen gas flow and examined by cyclic voltammetry (CV). The CVs have been recorded in the double layer potential range of the glassy carbon electrode (-1.1 to +1.3 V, under these experimental conditions). When the as-prepared CTAB-AuNRs are studied, no electrochemical signals are obtained, probably due to the presence of CTAB in such as high concentration (~ 0.1 M) that would be adsorbed and prevent the observation of any event on the electrode surface. However, after lowering the CTAB concentration, the electrochemical signals corresponding to the oxidation (at potentials higher than + 0.6 V) and reduction (at ~ + 0.5 V) of the nanorod gold surface atoms, were observed. Figure 2 shows the CV obtained for CTAB-AuNRs that have been drop-casted from a solution of CTAB-AuNRs that are in equilibrium with 2 mM CTAB. Moreover, an additional pair of sharp peaks, in the double layer region of the gold electrochemical profile were observed (Figure 2). These also stand out from those observed on a clean glassy carbon surface under the same experimental conditions. These peaks appear at + 0.26 and + 0.13 V in the anodic and cathodic scans, respectively, and they are not observed in similar experiments carried out with a gold electrode in the presence of 2 mM CTAB.

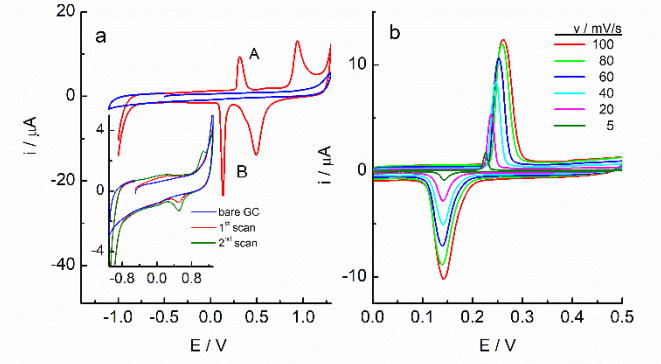

Figure 2. (a) CVs of a bare (——) and a modified glassy carbon electrode with CTAB-AuNRs (——) in a 50 mM sodium phosphate solution at pH 7.4; Insert: CVs taken under similar conditions but modified with MUA-AuNRs. (b) VCs in the potential range of the peaks A and B at different scan rates.

This suggests that they must be due to adsorbed CTAB on the AuNRs surface. To get more insight into the nature of these peaks, the potential scan is restricted from +0.0 to +0.5 V and the scan rate was changed (Figure 2b). At a first glance, the

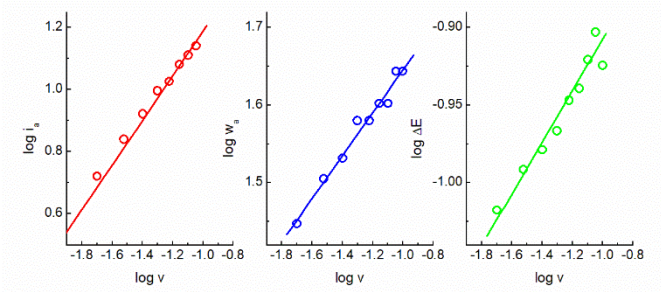

Figure 3. Logarithmic plots of the anodic intensity (i_a), peak half width (w_a) and anodic to cathodic potential peak difference (ΔE) against the scan rate.

peaks seem to behave similarly to those of reversible processes involving surface adsorbed molecules with strong lateral interactions.[41] However, for these processes, the half-widths of the peaks are independent of the scan rate, whereas the peaks observed in our system decrease with decreasing scan rate (Figure 3).[42] Moreover, even at the lower scan rate (5 mV/s), the peaks showed hysteresis (E_c = + 0.22 and E_a = + 0.14, with ΔE = 80 mV) that increases with the scan rate (Figure 3). This

behavior is typical of a two-dimensional phase transition phenomenon that can take place when the adsorbed molecules experience a conformational change from an ordered to either a disordered or a less ordered phase.[43] The theoretical predictions for these processes have been established and it follows a logarithmic linear variations of the peak current (i_a, i_c), half-width (w_a, w_c) and the potential difference between anodic and cathodic peaks (ΔE) versus the scan rate (v), being these variations with v^x, v^{1-x} and v^{1-x}, respectively (and, x = 0.6).[43] The slopes obtained for the variations of log i_a, log w and log ΔE vs log v (Figure 3) are 0.71, 0.27 and 0.2, respectively. They are very close to the theoretical predicted values and, therefore, in agreement with the hypothesis of the occurrence of a two-dimensional phase transition.

These electrochemical results can be explained by taking into account the Raman spectroscopy findings [6] stablishing that the CTAB molecules form a bilayer oriented in a perpendicular conformation to the AuNR surface when the concentration of CTAB in solution is high, but becoming disorganized when the concentration is lower than 2 mM. This concentration is close to the CTAB critical micellar concentration and, when the solution concentration is lower, the dynamic equilibrium required removes molecules from the bilayer leading to destabilization and the loss of its integrity.[6] In the present electrochemical experiment the CTAB solution concentration was 2 mM that is considered enough to maintain de bilayer integrity. Initial applied potentials are negative, hence the electrode charge, are negative and can produce some attractive forces on the positively charged heads of CTA^+ that should help to keep the layer organization. When the potentials are swept to positive values up to the potential of zero charge (pzc), from which the electrode would acquire a positive charge, the molecules can experience some repulsion forces provoking some disorganization in the layer. In the reverse scan, the organization of the layer is newly obtained upon reaching the appropriate potential values. The higher charging current at potentials higher than these peaks, in comparison with that at lower potentials, confirms this hypothesis (an estimation of the double layer capacity gives a value that is 8 % higher at potentials lower than the peaks in respect to that at lower potentials). The insert of Figure 2a shows the results of a parallel experiment where now MUA-AuNRs were used. In the first anodic scan, the electrochemical signal is not much different from that of the bare glassy carbon electrode and the oxidation of the gold surface is inhibited by the presence of the MUA-SAM. Well organized SAMs protect the gold surface from oxidation but, if the potential goes to higher values, they can be oxidatively desorbed.[44] The peak observed in the reverse scan should be due to the reduction of the gold nanorod surface atoms that became oxidized at the highest potentials experimented in the direct scan. Now, in a second scan, the electrochemical profile of a gold surface is evident, in agreement with the potential induced desorption of the complete MUA-SAM from the AuNRs surface. It is interesting to highlight that the peaks A and B are now absent, indicating the elimination of CTAB bilayer from the AuNRs surfaces upon ligand exchange procedure.

Characterization by XPS spectroscopy.

To get more insight into the extent of the ligand exchange processes, the different AuNRs have been analyzed by XPS spectroscopy (Figure 4). The samples to be studied were prepared by drop-casting a small volume of the nanorod suspensions in quartz crystal substrates that were left overnight for water evaporation. The low-resolution spectra show signals at 102, 154, 285 and 533 eV that correspond to the Si 2p, Si 2s, C 1s and O 1s components, respectively, of the quartz crystal together with signals corresponding to the AuNRs. Thus, the Au 4f doublet at 84 and 87 eV is observed in agreement with the presence of AuNRs on the surface.

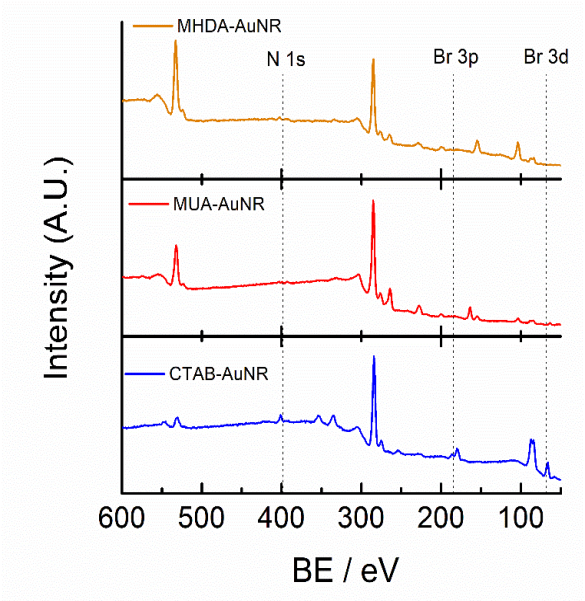

Figure 4. XPS low resolution spectra of AuNRs modified with different films. The dotted lines indicate the signals corresponding to Br 3d, Br 3p and N 1s.

The CTAB-AuNRs spectra shows the signals corresponding to Br (Br 3p at 179/187 and Br 3d at 66 eV), together with the N 1s signal at 400 eV. These signals are absent in the MUA- and MHDA-AuNRs spectra indicating the disappearance of the CTAB bilayer from the AuNRs surfaces. This is better observed in the high-resolution spectrum recorded in the region of Br 3p (Figure 5A) for the three samples studied.[45] An additional evidence for the ligand exchange is the presence of the signal corresponding to S 2p centered at 162.4 eV that can be deconvoluted by a doublet (due to spin-orbit coupling separated by 1.2 eV and with an area ratio of 1:2) with maxima at 162.2 and 163.4 eV for the levels S $2p_{3/2}$ and S $2p_{1/2}$, respectively (Figure 5B).[46-49] The XPS signals for C 1s for CTAB-AuNRs (Figure 5C) and MUA-AuNRs (Figure 5D) show the component at 284.0 eV assigned to methylene groups of the alkane chains of the protective layers and the components of higher energies to the C atoms that are bound to more electronegative atoms such as N or O in CTAB and MUA, respectively.[50] Thus, the two components at 284.0 eV and 285.2 eV in CTAB-AuNRs are ascribed to the methylene carbons (C 1s (1)) and these bound to the quaternary ammonium N (C 1s (2)), respectively, whereas in MUA- or

MHDA-AuNRs, components at 284/285, 285.6/286.3 and 287.5/288 eV are ascribed to alkane chain (C 1s (1)), CH_2-O groups (C 1s (2)) and C=O (C 1s (3)), respectively.

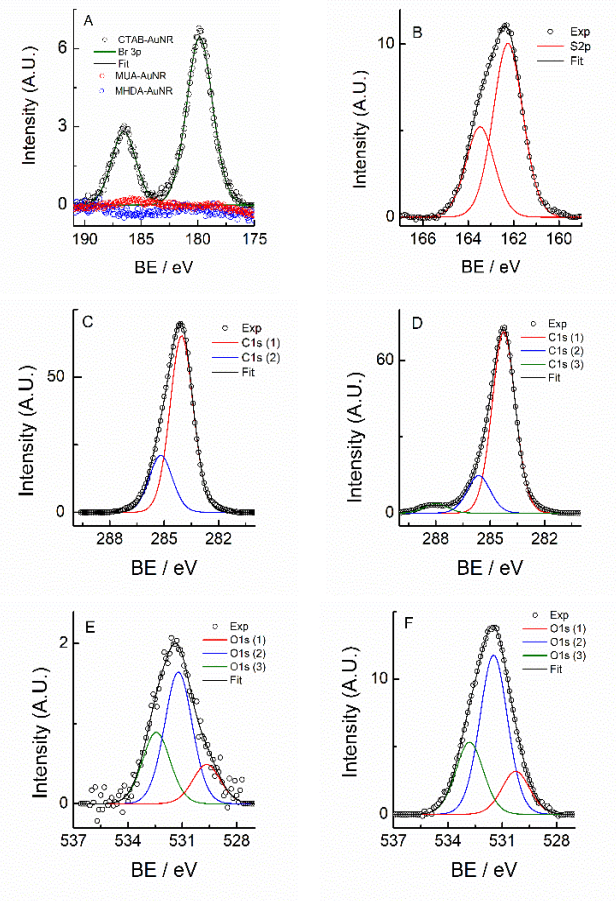

Figure 5. XPS high resolution spectra recorded in the energy region corresponding to (A) CTAB-, MUA- and MHDA-AuNRs: Br 3p; (B) MUA-AuNRs: S 2p; (C) CTAB-AuNRs: C 1s, (D) MUA-AuNRs: C 1s; (E) CTAB-AuNRs: O 1s; (F) MUA-AuNRs: O 1s.

The spectra of O 1s are deconvoluted with three components with values of 529.7/531.2, 531/533 and 532.4/533.8 eV (Figure 5E, F). The two first components are usually ascribed to O atoms in groups C-O and C=O, whereas the component at higher binding energy should correspond to O atoms of the water molecules adsorbed in the layer.[51] In the case of CTAB-AuNRs, the observed peak can also be deconvoluted by three components. Although the relative area of this signal, in comparison to the cases of MUA- and MHDA-AuNRs, is very low, they indicate the presence of some oxygen containing molecules in the CTAB bilayer. The existence of water molecules trapped near the tetramethylammonium heads as well as the observation of the O atoms of the SiO_2 quartz crystal substrate that are normally observed at 532.7 eV [52] cannot be discarded. In fact, the later signal can also be convoluted with the assigned water peak in the spectra of MUA- and MHDA-AuNRs. In short, the absence of Br 3p and the presence of S 2p peaks in the spectra of MUA- and MHDA-AuNRs are the features that allow us to conclude that the ligand exchange procedure has been successful.

FT-IR spectroscopy.

FTIR spectroscopy allows us to know the composition as well as the conformation and organization of the molecules in the layers built on the nanomaterial surfaces.

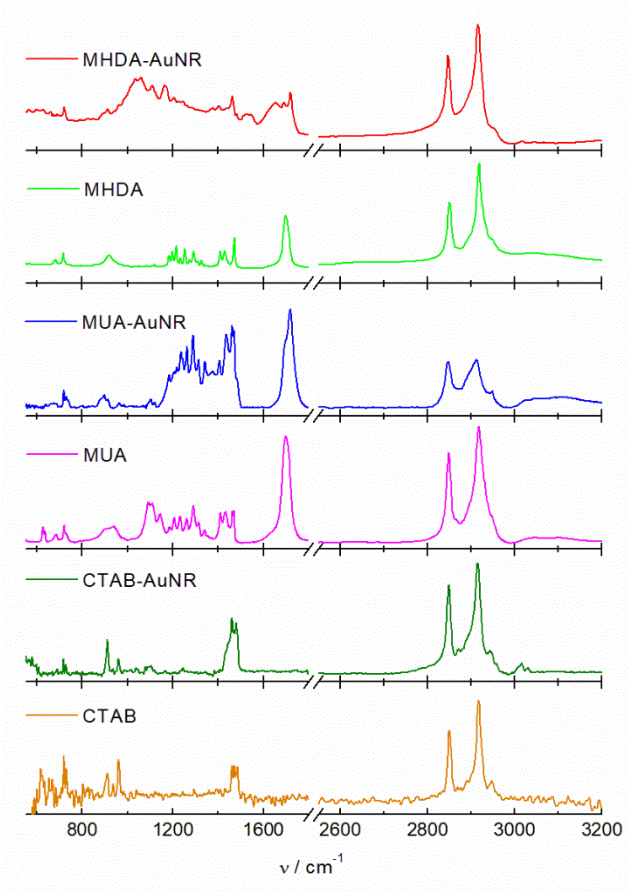

Figure 6. FT-IR spectra of *CTAB, CTAB-AuNRs, MUA, MUA-AuNRs, MHDA and MHDA-AuNRs.*

Figure 6 shows the spectra for the studied systems together with those of the starting compounds. The high frequency region is characterized by the presence of peaks due to the asymmetric and symmetric stretching modes of the methylene groups at 2920 and 2850 cm^{-1}, respectively. These values are typical of well-organized methylene chains in self-assembled monolayers and shifts to higher energies have been observed as the Van der Waals interactions between the alkyl chains decrease.[53] However, for the different AuNRs examined, a small shift to lower energies are observed in comparison to the free compounds indicating a good organization of the molecules upon adsorption on the nanorod surface. The most outstanding features to highlight and evidence the ligand exchange of CTAB by MUA or MHDA molecules are on the one side, the disappearance of the C-N^+ stretching at 960, 938 and 908 cm^{-1} that are transformed in two bands at 960 and 911 cm^{-1} in the CTAB-AuNRs spectrum and on the other the appearance of the band at around 1700 cm^{-1} typical of the carbonyl groups.[2] A closer look of this later band in the spectra of the different species allows us to get more insight into the structure of the layers upon exchange. In Figure S3, a comparison of these peaks

after deconvolution by using Lorentzian curves is presented. The band at 1700 cm^{-1} observed for free MUA molecules shows a light asymmetry that invite to make a deconvolution of the signal into two peaks. Thus, peaks at 1695 and 1720 cm^{-1} with area ratios of 77 and 23 %, respectively, are obtained. The first signal can be ascribed to carbonyl groups involved in hydrogen bonds and the second one to free species. In the case of MUA-AuNRs, a different shape is clearly seen that can be decomposed into two bands with similar characteristics of the free MUA molecules but with a different area ratio of 21 and 79 % at 1695 and 1720 cm^{-1} respectively. This indicates an important decrease in hydrogen bonds content when the MUA are bound to the nanorod surface.

In the case of MHDA, the changes observed in the analysis of the peak in this energy region are somehow more complex (Figure S3). The single peak observed in the free molecules at 1700 cm^{-1} is now deconvoluted into four signals at 1720, 1690, 1654 and 1618 cm^{-1}. The peak at lower energy has been assigned to residual water that can be trapped into the monolayer [54] and these at higher frequencies should be ascribed to a mixture of different hydrogen bonded and nonbonded species that are represented in a similar proportion. Whereas the higher energy peak is assigned to free carbonyl groups, the two at lower energy have been assigned either to hydrogen bonds formed between neighboring groups or formed in a head-to-head fashion probably between MHDA molecules grafted in different AuNRs. Finally, the higher number of signals in the low frequency region precludes further analysis at this level of resolution. In the end, FTIR spectra of the different organic layers covering the AuNR surfaces inform, not only on the effective exchange process but also, on the structural organization of the molecules that could explain in some way the different stability of MUA- and MHDA-AuNRs in solution.

Raman spectroscopy.

Additional information can be obtained from Raman spectroscopy (Figure 7). The presence of a nanostructured substrate, as it is the case for the AuNRs, induces an increase on the intensity of the Raman signals due to a SERS effect that is absent in the spectra taken for the free ligands. The band at 170 cm^{-1} that is observed in the CTAB-AuNRs spectrum, but is absent for the free CTAB, [31] corresponds to the Au-Br bond,[55] which existence would allow the interaction of the CTA^+ chains through the head group with the Br^- covered surface. Moreover, the collapse of the set of bands at 748, 758 and 770 cm^{-1} of the stretching vibrations of the trimethylammonium group in a broader band at 760 cm^{-1} can indicate the loss of mobility of these bonds upon interaction with the surface.[6, 56] Other bands characteristics of longer alkane chains are the C-C skeleton vibrations at 1070 and 1144 cm^{-1} and these due to CH_2 groups at 1295, 1493, 1447, 1464 and 1481 cm^{-1}. Most of these bands do not appear in CTAB-AuNRs probably due to overlapping and the lack of resolution. In the high frequency region, the symmetric and asymmetric CH_2 stretches at 2850 and 2880 cm^{-1} and CH_3 at 2930 and 2950 cm^{-1}, respectively show a significant change in their ratios from the free and bound CTAB, indicating the different conformation and environment of the chains. Finally, the band at 3040 cm^{-1} characteristic of the asymmetric N-C-H stretch can also be seen.[56]

The MUA Raman spectrum is also compared with the SERS spectrum of MUA-AuNRs. The vibrations of the bonds that are sensitive to the adsorption of the molecule to the metal surface are the $\nu(C\text{-}S)_T$ at 730 cm^{-1} and $\nu(C\text{-}C)_T$ at 1099 cm^{-1} and, they can be used to characterize the adsorption process, the conformational state of the molecules adsorbed on the surface and the *trans* character of the molecular chains.[57-61] These bands appear in the SERS spectrum (710 and 1102 cm^{-1}) while those corresponding to the gauche conformation are absent. On the other hand, the Raman spectrum of MUA shows the presence of the bands at 2549 and 2575 cm^{-1} assigned to the S-H stretch.[61] These bands completely disappear in the SERS spectrum indicating that the MUA molecules bind preferentially through the thiol group. The band ν(COOH) is observed in the Raman spectrum at 908 cm^{-1} and proportionally decreases and changes to 926 cm^{-1}. This fact together with the absence of the band at 1631 cm^{-1} (C=O group) indicate the presence of carboxylate groups in the MUA-AuNRs. It has been described that the distance separating this group from the surface that provokes the SERS effect makes this bond to be of lower intensity, even disappearing from the spectrum.[60] On the other hand, the Au-Br bond at 175 cm^{-1} completely disappears in the MUA-AuNRs and this fact together with the absence of the band at 760 cm^{-1} due to the trimethyl ammonium of the CTAB, indicates a complete exchange of the CTAB by MUA molecules.

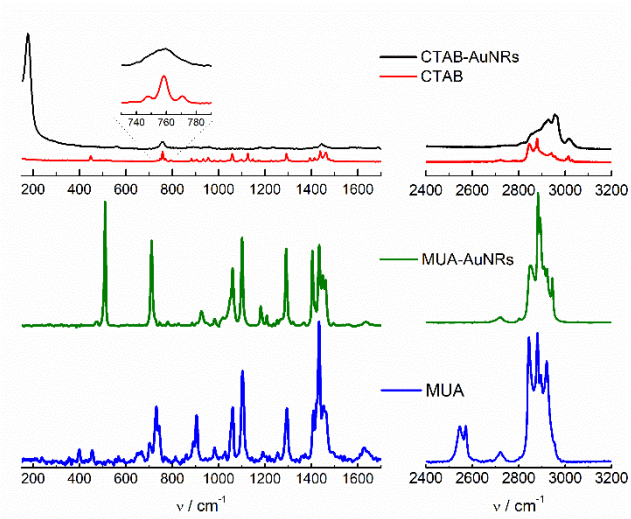

Figure 7. Raman spectra of *CTAB (—), MUA (—) and SERS spectra of CTAB-AuNRs (—) and MUA-AuNRs (—).*

Stability of CTAB-, MUA- and MHDA-AuNRs in aqueous solutions

The use of these nanomaterials in fields such as biomedicine requires a knowledge on the stability in aqueous media. First at all, it is noteworthy that the stability of these modified AuNRs, either with MUA or MHDA is excellent. Figure S2 (Supporting information) shows UV-visible spectra recorded for the just exchanged samples presenting this exchange and

the same samples a year later. As it can be seen, the spectra do not show any significant variation, which is consistent with a scenario high stability of the AuNRs protected by carboxy-terminated alkanethiols. We have carried out a study on the stability in aqueous solutions of different pH to get information on the possible aggregation behavior of these AuNRs (Figure 8).

To start with, the CTAB-AuNRs have been examined by changing the pH of the media by adding either HCl or NaOH in the presence of 2 mM CTAB to maintain the integrity of the bilayer. The shape of these spectra does not change in the interval 3 < pH < 10 but, at higher values, a blue shift of the longitudinal band of around 15 nm, in parallel with a decrease in absorbance can be observed (Figure 8A). The transverse band shows a similar behavior and it is accompanied by a red shift of the wavelength.[62]

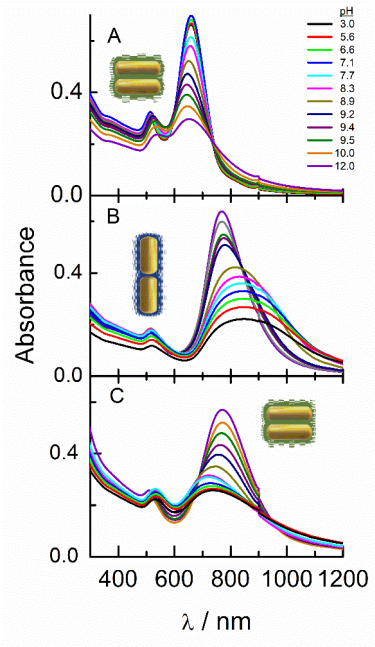

Figure 8. UV-visible-NIR spectra of the (A) CTAB-, (B) MUA- and (C) HDMA-AuNRs as a function of solution pH.

Figure 9 shows the comparison of the displacements of the longitudinal and transverse bands in respect to the values of these magnitudes at pH 10. pH 10 was selected after a preliminary study that shows that the three modified AuNRs studied are colloidally stable under these conditions.

As it is described in the Experimental section, the exchange of CTAB by MUA and MHDA is carried out in an alkaline media, being these the optimum conditions to obtain the highest stability, probably due to the repulsion produced by both, the positive charges of the CTA^+ and the negative ones of the carboxylate groups of the protective SAM. To attain this situation, it is necessary to get the ligand exchange in a concerted way that avoids the loss of stability in solution. The spectra obtained for MUA-AuNRs at different pHs are shown in Figure 8B. it can be observed that the maximum wavelength of the longitudinal and transverse bands, as well as its absorbance, do not change upon decreasing the pH up to neutral medium (pH ~ 7). When the medium becomes more acidic, a small displacement of the maximum wavelength together with a widening of the half width band are obtained that become more important at lower pHs. These data can be fitted to sigmoidal curves with inflections at pH 4.9 and 7.0. These values can be associated with apparent dissociation pK_a of the carboxylate groups on the AuNR surface. The pK_a of carboxylate groups higher than those obtained for the free molecules in solution have been observed in carboxylic terminated SAMs and have been explained by the retention of the bound hydrogen due to the formation of hydrogen bonds between neighboring groups in the monolayer.[63-65]

The features observed in the present study differ from early reported results[62, 66-68] that studied the assembly of CTAB-AuNRs in the presence of some bifunctional molecules that drive the nanorods to end-to-end or side-by-side interactions depending on its concentration. Although, in some cases these bifunctional molecules are tightly bound to the gold surface, they are always in equilibrium with those free in solution that help in the reversible assembly behavior observed. In the present study, we have used conditions that pursuit the absence of free molecules and the formation of compact monolayers on the nanorod surfaces. Thus, the equilibrium is driven by the state of the bound molecules that are strongly dependent on the configuration they adopt in the monolayer.

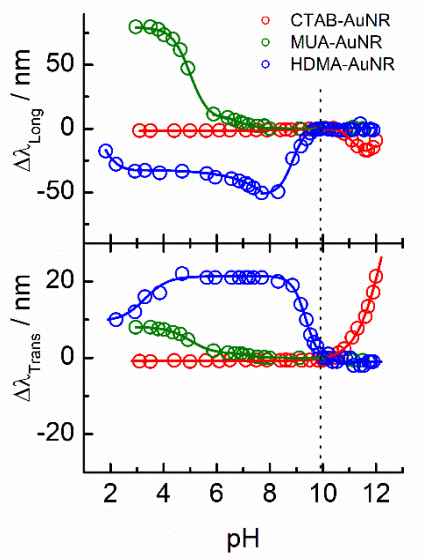

Figure 9. Wavelength displacements for the longitudinal and transverse bands for the CTAB-, MUA- and MHDA-AuNRs in respect to the value obtained at pH 10 as a function of the solution pH.

This fact includes the possibility of intermolecular interactions not only inside the monolayer but also, between molecules of different AuNRs. Thus, it can be thought that the displacement of wavelength observed can be due to the interaction between different AuNRs when some of the carboxylates become protonated. At lower pH, the protonation of the carboxylate groups at the typical pk_a value, induces a higher tendency to aggregation, firstly in an *end-to-end* fashion and finally with the formation of bigger aggregates that should

start to precipitate, as it is suggested by the decrease in absorbance concomitant with the red shift displacement. These results can be correlated with the FTIR results described above that show that, while the carboxylic groups of free MUA molecules are mostly involved in H-bond, in the MUA-AuNRs only 20% of these are participating in these interactions, the rest of groups remaining as non-interacting.

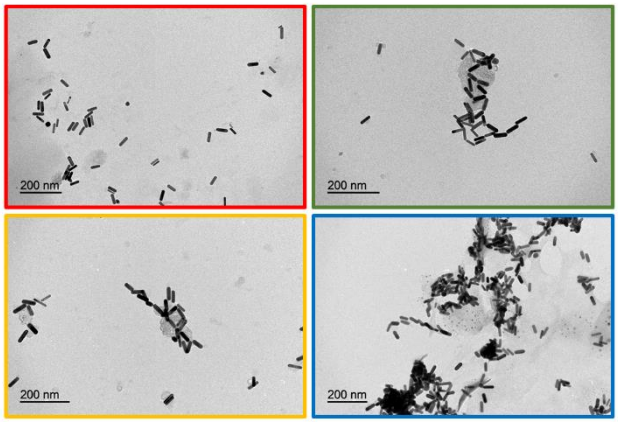

Figure 10. TEM images of MUA-AuNRs from solutions at different pH: 11.2, 7.5, 6.2, and 3.3.

Finally, the stability of the MHDA-AuNRs in alkaline media is somewhat different to that for the MUA-AuNRs. At pH < 10 a strong blue shift in parallel with a decrease in absorbance with an inflection near pH 8.5 is observed. The transverse band shows a red shift in a symmetric fashion with the longitudinal band, in agreement with *side-by-side* interactions. Again, a displacement of the carboxylic groups pK_a to higher values is observed but in a different way that occurs in the case of MUA-AuNRs. This effect must be related to the longer alkane chain that can form a more compact monolayer where the terminal groups can interact more strongly. In fact, the *side-by-side* configuration implies that the terminal carboxylic groups in the side of the rods remain undissociated and facilitate the interaction by hydrogen bonds. This fact can also be explained by the FTIR results that show the existence of three different configurations of the carboxylic groups, non-bonded and forming H bonds with its neighbors or with the carboxylic groups anchored to other AuNRs.

These effects can be observed in the TEM images obtained at different pH values. The photographs shown in Figures 10 and 11 have been obtained by dropping solutions of MUA- or MHDA-AuNRs in the carbon grids and allowing them to dry overnight. Although this procedure may be masked by the action of capillary forces and not provide an accurate picture of the processes that are taking place in solution,[62] the images can serve as a complement of the conclusions drawn from UV-visible spectra. As it can be observed, in the case of MUA-AuNRs the *end-to-end* interactions occur in parallel with the first inflection observed in Figure 9 for the wavelength displacement. At lower pHs, the interactions increase up to higher aggregates can be observed (Figure 10).

The TEM images obtained for the MHDA-AuNRs at different pH also agree with the above described behavior (Figure 11). It can be observed that, in alkaline media, the MHDA-AuNRs are very well separated whereas in the image obtained for pH 8.8, some *side-by-side* aggregates start to form. By lowering pH even further the *side-by-side* aggregation is maintained even at the lowest pH of 3.4 where the aggregates are much bigger.

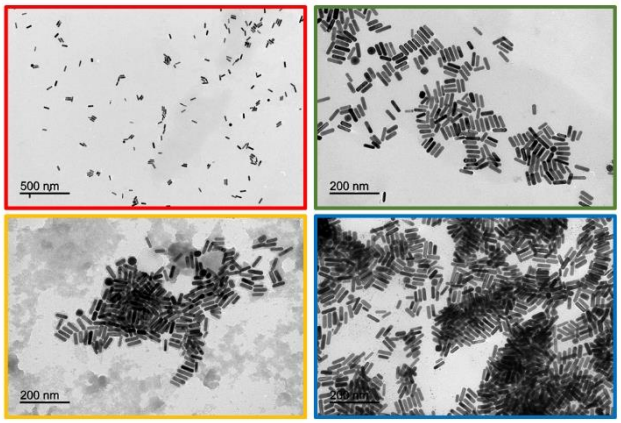

Figure 11. TEM images of MHDA-AuNRs from solutions at different pH: 11.8, 8.5, 7.5 and 3.3.

The different behavior observed for the MUA- and MHDA-AuNRs is intriguing but the explanation for this different organization can be found on the different conformation of the carboxy-terminated molecules in the nanorod surface depending on the chain length. Thus, it can be said that the longer chain length of the MHDA induces the formation of a well-packed monolayer that is further stabilized by hydrogen bonds and resists higher pH without dissociation. In the case of MUA-AuNRs, the carboxylic terminal groups, although must be in a similar configuration to that of MHDA-AuNRs, have preference for the *end-to-end* and not for the *side-by-side* interactions, probably due to a more loosely configuration that allows dissociation of these groups. These findings have an important implication for the potential application of these AuNRs in biological systems. Whereas the MUA-AuNRs keep stable in solution under physiological conditions, the MHDA-AuNRs present a tendency to aggregation that may result not appropriate for its use under these conditions.

3. Conclusions

The difficulties to completely understand and carry out ligand exchange on AuNRs are mainly due to the presence of the CTAB bilayer that comes from its use as morphology-guiding surfactant.[69] Although many reports have been published on this topic, there is still a need to find new methods for the complete removal of CTAB from the surface of AuNRs to realize the potential of gold nanorods towards critical biological applications.[31] In this work we have described a methodology for CTAB exchange from the AuNR surfaces that is based on the knowledge of the stability of the AuNRs in aqueous solutions. Two points are taken into account: on the one side, the concentration of surfactant is chosen at 2 mM as this concentration maintains the bilayer but allows the exchange by mercaptoderivative molecules that can strongly bind to the gold

surface; on the other, keeping the pH of the solution to a value where both the starting CTAB-AuNRs and the resulting modified specimens are stable. The characterization of the different species by experimental techniques that inform about *the structure and conformation of the molecules in the layer* allows us to conclude that this methodology can be translated to the exchanging of any molecule if the stability conditions are known. Finally, the different behavior of the modified AuNRs in aqueous solutions gives us some clues about the possibility of applications in living systems.

Scheme 2. Exchange of CTAB by MUA in the surface of the AuNRs.

4. Experimental

Chemicals.

Cetyltrimethylammonium bromide (CTAB), 11-mercaptoundecanoic acid (MUA), 16-mercaptohexanoic acid (MHDA), Sodium borohydride ($NaBH_4$), Silver nitrate ($AgNO_3$), ascorbic acid (AA) were from Sigma-Aldrich-Merck. The rest of reactants were of analytical grade. All solutions were prepared with deionized water produced by Millipore system.

Synthesis of the CTAB-AuNRs.

The AuNRs have been prepared by a seed-mediated procedure.[14-16] In a typical synthesis, the seeds were produced by mixing 5 mL of a 0.2 M CTAB solution with 5 mL of 0.5 mM $HAuCl_4$ under vigorous stirring. To this solution, 0.6 mL of 0.01 M $NaBH_4$ (in an ice bath) were added, producing a fast color change. This mixture was kept under stirring during 2 min at 25 ºC to get the gold seeds. The growth solution was formed by mixing 475 mL of 0.1 M CTAB solution with 5 mL of 0.01 M of $AgNO_3$. This mixture was maintained under soft stirring while 25 mL of 0.01 M $HAuCl_4$ and 2.75 mL of a recently prepared 0.1 M AA solutions were sequentially added. The addition of the weak reductant AA results in the formation of Au(I), that is evidenced by a color change from dark yellow to a transparent solution. Now, 0.6 mL of the seed solution were added to the growth solution, keeping the temperature at 27 ºC. The solution color changed in 10-20 min to a greenest or brown color depending on the final size of the CTAB-AuNRs.

Surface modification of the AuNRs.

The CTAB-AuNRs solution obtained by this synthetic procedure contains a high CTAB concentration (~0.1 M). To proceed with the ligand exchange protocol, it was necessary to decrease the surfactant concentration, and this was made by carrying out several centrifugation cycles (10.000 rpm during 20 min) and dispersing the precipitate in a 2 mM CTAB solution to avoid the aggregation of the AuNRs. The solution was then mixed with an amount of the thiol derivative (MUA or MHDA) that was twice the theoretically necessary to completely cover the AuNRs surface, based on the size of the AuNRs determined by TEM, and the fingerprint of the mercaptoderivative molecules.[63] The pH of the mixture was maintained to 10 by adding NaOH and was kept overnight under mild stirring. After this step, the excess of reactants was removed by several dialysis cycles against 10 mM NaOH solutions (Scheme 2).

Experimental techniques.

The absorbance spectra were recorded using a Jasco V-670 UV-vis-NIR spectrophotometer. ATR infrared spectra were recorded on a JASCO 6300 FTIR single (He-Ne) laser beam spectrometer and the data were acquired by the integrated software (Spectra Manager). A variable angle specular reflectance accessory (Pike Technologies-VeeMAX^{TM}) assembled in the FTIR spectrometer compartment enabled samples to be analyzed at different beam incident angles. A germanium crystal with an orientation of 60º was used. The spectra were collected using an uncooled single element DTGS–detector. Then, a total of 256 scans were averaged at a spectral resolution of 2 cm^{-1} in the frequency window of 4000–1000 cm^{-1}. Prior to the measurements, the interferometer and the sample compartments were purged with a dry and free CO_2 air flux of 8 L/min, supplied by a compressed air adsorption dryer (K-MT LAB, Parker/Zandet GmbH&Co.KG).

TEM images were obtained with a JEOL JEM 1400 instrument (Servicio Central de Apoyo a la Investigación (SCAI) Universidad de Córdoba) operating at 80–120 kV and analyzed using Image Pro Plus software. Samples were prepared by casting and evaporating a droplet of nanomaterial solutions onto Formvar-coated Cu grids (400 mesh, Electron Microscopy Sciences).

Electrochemical experiments were performed using an Autolab (Ecochemie model Pgstat20) instrument attached to a PC with proper software (GPES and FRA) for the total control of the experiments and data acquisition. A conventional three electrode cell comprising a platinum coil as the counter electrode, a saturated calomel electrode as the reference electrode and a glassy carbon (GC) as the working electrode were used. Before each electrochemical measurement, the electrode was polished by using alumina slurries and sonicated in an ultrasound bath. After that, the clean electrode was cycled in a potential range from −1.1 to +1.1 V in 50 mM phosphate buffer at pH 7.4 up to a reproducible profile typical of a clean GC electrode was obtained. This surface treatment was the most appropriate to produce a surface that is clean, ordered and highly reproducible.

X-ray photoelectronic spectroscopy (XPS) (Servicio Central de Apoyo a la Investigación (SCAI) Universidad de Córdoba) analyses were performed with a SPECS Phoibos 150 MCD spectrometer using non-monochromatized (12 kV, 300 W) Mg KR radiation (1253.6 eV). The samples were mounted on a steel

sample holder and introduced directly into the XPS analytical chamber. The working pressure was < 5×10^{-9} Pa. The spectra were collected using a take-off angle of 45° with respect to the sample surface plane. The spectrometer was calibrated assuming the binding energy (BE) of the Au $4f_{7/2}$ line at 84.0 eV. The standard deviation for the BE values was 0.2 eV. Survey scans were run in the 0 – 1100 eV range (pass energy=60 eV), while detailed scans were recorded for the Br 3p, S 2p, C 1s, and O 1s regions. The analysis involved Shirley background subtraction, and whenever necessary, spectral deconvolution was carried out by nonlinear least-squares curve fitting, adopting a Gaussian sum function.

Raman and Surface Enhanced Raman Spectroscopic (SERS) measurements were performed with a HORIBA Jobin Yvon LabRaman spectro-graph with a holographic grating of 600 $g \cdot mm^{-1}$. The excitation line was provided by a 17 mW He-Ne laser at 633.0 nm. The laser beam was focused through an Olympus 50x long working distance objective (0.5 NA) into a 2 μm spot at the electrode surface. Signal averaging of two spectra with spectrometer resolution better than 3 cm^{-1}, 60 s acquisition time each, was performed.

Conflicts of interest

There are no conflicts to declare.

Acknowledgements

We thank the Ministerio de Economía y Competitividad (MINECO) (Projects CTQ2014-60227-R and CTQ-2015-71955-REDT Network of excellence Sensors and Biosensors) and University of Córdoba for financial support of this work.

5. References

1. J. Perez-Juste, I. Pastoriza-Santos, L. M. Liz-Marzan and P. Mulvaney, *Coord. Chem. Rev.*, 2005, **249**, 1870-1901.
2. B. Nikoobakht and M. A. El-Sayed, *Langmuir*, 2001, **17**, 6368-6374.
3. T. K. Sau and C. J. Murphy, *Langmuir*, 2005, **21**, 2923-2929.
4. L. Wang, X. Jiang, Y. Ji, R. Bai, Y. Zhao, X. Wu and C. Chen, *Nanoscale*, 2013, **5**, 8384-8391.
5. C. R.-K. Betty, L. R. Bickford, C. M. Payne, E. S. Day, L. J. E. Anderson, M. Zhong, S. Lee, K. M. Mayer, T. Zal, L. Adam, C. P. N. Dinney, R. A. Drezek, J. L. West and J. H. Hafner, *Nanotechnology*, 2009, **20**, 434005.
6. S. Lee, L. J. E. Anderson, C. M. Payne and J. H. Hafner, *Langmuir*, 2011, **27**, 14748-14756.
7. C. J. Murphy, L. B. Thompson, A. M. Alkilany, P. N. Sisco, S. P. Boulos, S. T. Sivapalan, J. A. Yang, D. J. Chernak and J. Y. Huang, *J. Phys. Chem. Letters*, 2010, **1**, 2867-2875.
8. H. Chen, L. Shao, Q. Li and J. Wang, *Chem. Soc. Rev.*, 2013, **42**, 2679-2724.
9. D. Nepal, K. Park and R. A. Vaia, *Small*, 2012, **8**, 1013-1020.
10. B. Nikoobakht, J. P. Wang and M. A. El-Sayed, *Chem. Phys. Letters*, 2002, **366**, 17-23.
11. D. K. Smith, N. R. Miller and B. A. Korgel, *Langmuir*, 2009, **25**, 9518-9524.
12. J. E. Millstone, W. Wei, M. R. Jones, H. Yoo and C. A. Mirkin, *Nano Letters*, 2008, **8**, 2526-2529.
13. N. Garg, C. Scholl, A. Mohanty and R. Jin, *Langmuir*, 2010, **26**, 10271-10276.
14. A. Gole and C. J. Murphy, *Chem. Mater.*, 2004, **16**, 3633-3640.
15. C. J. Murphy, T. K. Sau, A. M. Gole, C. J. Orendorff, J. Gao, L. Gou, S. E. Hunyadi and T. Li, *J. Phys. Chem. B*, 2005, **109**, 13857-13870.
16. B. Nikoobakht and M. A. El-Sayed, *Chem. Mater.*, 2003, **15**, 1957-1962.
17. V. Sebastián, S.-K. Lee, C. Zhou, M. F. Kraus, J. G. Fujimoto and K. F. Jensen, *Chem. Commun.*, 2012, **48**, 6654-6656.
18. G. Grochola, I. K. Snook and S. P. Russo, *J. Chem. Phys.*, 2007, **127**.
19. K. Park, L. F. Drummy, R. C. Wadams, H. Koerner, D. Nepal, L. Fabris and R. A. Vaia, *Chem. Mater.*, 2013, **25**, 555-563.
20. S. Si, C. Leduc, M. H. Delville and B. Lounis, *Chemphyschem*, 2012, **13**, 193-202.
21. X. Ye, L. Jin, H. Caglayan, J. Chen, G. Xing, C. Zheng, V. Doan-Nguyen, Y. Kang, N. Engheta, C. R. Kagan and C. B. Murray, *ACS Nano*, 2012, **6**, 2804-2817.
22. E. Carbo-Argibay, B. Rodriguez-Gonzalez, S. Gomez-Grana, A. Guerrero-Martinez, I. Pastoriza-Santos, J. Perez-Juste and L. M. Liz-Marzan, *Angew. Chem.*, 2010, **49**, 9397-9400.
23. T. Placido, R. Comparelli, F. Giannici, P. D. Cozzoli, G. Capitani, M. Striccoli, A. Agostiano and M. L. Curri, *Chem. Mater.*, 2009, **21**, 4192-4202.
24. M. Liu and P. Guyot-Sionnest, *J. Phys. Chem. B*, 2005, **109**, 22192-22200.
25. F. Hubert, F. Testard and O. Spalla, *Langmuir*, 2008, **24**, 9219-9222.
26. L. M. Moreau, M. R. Jones, E. W. Roth, J. Wu, S. Kewalramani, M. N. O'Brien, B.-R. Chen, C. A. Mirkin and M. J. Bedzyk, *Nanoscale*, 2019, **11**, 11744-11754.
27. E. Reyes, R. Madueño, M. Blazquez and T. Pineda, *J. Phys. Chem. C*, 2010, **114**, 15955-15962.
28. F. Scaletti, C. S. Kim, L. Messori and V. M. Rotello, *MethodsX*, 2014, **1**, 118-123.
29. L. J. Su, S. Hu, L. Zhang, Z. R. Wang, W. P. Gao, J. Yuan and M. H. Liu, *Small*, 2017, **13**.
30. Q. Shou, M. Ebara, J. Wang, Q. Wang, X. Liang, H. Liu and T. Aoyagi, *Appl. Surf. Sci.*, 2018, **457**, 264-270.
31. J. He, S. Unser, I. Bruzas, R. Cary, Z. W. Shi, R. Mehra, K. Aron and L. Sagle, *Colloids Surf. B*, 2018, **163**, 140-145.
32. A. Gole and C. J. Murphy, *Chem. Mater.*, 2005, **17**, 1325-1330.
33. L. Vigderman, B. P. Khanal and E. R. Zubarev, *Adv. Mater.*, 2012, **24**, 4811-4841.
34. L. H. Dubois and R. G. Nuzzo, *Annu. Rev. Phys. Chem*, 1992, **43**, 437-463.
35. A. Wijaya and K. Hamad-Schifferli, *Langmuir*, 2008, **24**, 9966-9969.
36. L. Vigderman, P. Manna and E. R. Zubarev, *Angew. Chem.*, 2012, **51**, 636-641.
37. B. Thierry, J. Ng, T. Krieg and H. J. Griesser, *Chem. Commun.*, 2009, 1724-1726.
38. A. J. Viudez, R. Madueno, T. Pineda and M. Blazquez, *J. Phys. Chem. B*, 2006, **110**, 17840-17847.
39. A. J. Viudez, R. Madueno, M. Blazquez and T. Pineda, *J. Phys. Chem. C*, 2009, **113**, 5186-5192.
40. F. Canaveras, R. Madueño, J. M. Sevilla, M. Blazquez and T. Pineda, *J. Phys. Chem. C*, 2012, **116**, 10430-10437.
41. E. Laviron, in *Electroanalytical Chemistry*, ed. A. J. Bard, Marcel Decker, New York, 1982, vol. 12, p. 53.

42. L. M. Peter, J. D. Reid and B. R. Scharifker, *J. Electroanal. Chem.*, 1981, **119**, 73-91.
43. M. S. Maestre, R. Rodriguez Amaro, E. Munoz, J. J. Ruiz and L. Camacho, *J. Electroanal. Chem.*, 1994, **373**, 31-37.
44. D. Garcia-Raya, R. Madueno, J. Manuel Sevilla, M. Blazquez and T. Pineda, *Electrochim. Acta*, 2008, **53**, 8026-8033.
45. J. Cao, E. K. Galbraith, T. Sun and K. T. V. Grattan, *Sens Actuators B Chem.*, 2012, **169**, 360-367.
46. M. J. Hostetler, J. E. Wingate, C. J. Zhong, J. E. Harris, R. W. Vachet, M. R. Clark, J. D. Londono, S. J. Green, J. J. Stokes, G. D. Wignall, G. L. Glish, M. D. Porter, N. D. Evans and R. W. Murray, *Langmuir*, 1998, **14**, 17-30.
47. M.-C. Bourg, A. Badia and R. B. Lennox, *J. Phys. Chem. B*, 2000, **104**, 6562-6567.
48. K. Heister, M. Zharnikov, M. Grunze and L. S. O. Johansson, *J. Phys. Chem. B*, 2001, **105**, 4058-4061.
49. Y. Joseph, I. Besnard, M. Rosenberger, B. Guse, H.-G. Nothofer, J. M. Wessels, U. Wild, A. Knop-Gericke, D. Su, R. Schlögl, A. Yasuda and T. Vossmeyer, *J. Phys. Chem. B*, 2003, **107**, 7406-7413.
50. L. Costelle, M. T. Räisänen, J. T. Joyce, C. Silien, L.-S. Johansson, J. M. Campbell and J. Räisänen, *J. Phys. Chem. C*, 2012, **116**, 22602-22607.
51. X.-P. He, X.-W. Wang, X.-P. Jin, H. Zhou, X.-X. Shi, G.-R. Chen and Y.-T. Long, *J. Am. Chem. Soc.*, 2011, **133**, 3649-3657.
52. E. Görlich, J. Haber, A. Stoch and J. Stoch, *J. Solid State Chem.*, 1980, **33**, 121-124.
53. M. D. Porter, T. B. Bright, D. L. Allara and C. E. D. Chidsey, *J. Am. Chem. Soc.*, 1987, **109**, 3559-3568.
54. O. Gershevitz and C. N. Sukenik, *J. Am. Chem. Soc.*, 2004, **126**, 482-483.
55. E. Koglin, A. Tarazona, S. Kreisig and M. J. Schwuger, *Colloids* ***Surf*** *. A*, 1997, **123-124**, 523-542.
56. M. Tebbe, C. Kuttner, M. Männel, A. Fery and M. Chanana, *ACS Appl. Mater. Interfaces*, 2015, **7**, 5984-5991.
57. J. L. Castro, M. R. López-Ramírez, J. F. Arenas and J. C. Otero, *J. Raman Spectrosc.*, 2004, **35**, 997-1000.
58. B. Wrzosek, J. Bukowska and A. Kudelski, *J. Raman Spectrosc.*, 2005, **36**, 1040-1046.
59. C. Ma and J. M. Harris, *Langmuir*, 2012, **28**, 2628-2636.
60. F. C. Marques, G. P. Oliveira, R. A. R. Teixeira, R. M. S. Justo, T. B. V. Neves and G. F. S. Andrade, *Vib. Spectrosc.*, 2018, **98**, 139-144.
61. S. K. Tripathy and Y.-T. Yu, *Spectrochim Acta A Mol Biomol Spectrosc*, 2009, **72**, 841-844.
62. P. K. Jain, S. Eustis and M. A. El-Sayed, *J. Phys. Chem. B*, 2006, **110**, 18243-18253.
63. Z. Gonzalez-Granados, G. Sanchez-Obrero, R. Madueño, J. M. Sevilla, M. Blazquez and T. Pineda, *J. Phys. Chem. C*, 2013, **117**, 24307-24316.
64. A. R. Puente Santiago, T. Pineda, M. Blazquez and R. Madueño, *J. Phys. Chem. C*, 2016, **120**, 8595-8606.
65. A. R. Puente Santiago, G. Sánchez-Obrero, T. Pineda, M. Blázquez and R. Madueño, *J. Phys. Chem. C*, 2018, **122**, 2854-2865.
66. K. G. Thomas, S. Barazzouk, B. I. Ipe, S. T. S. Joseph and P. V. Kamat, *J. Phys. Chem. B*, 2004, **108**, 13066-13068.
67. Z. Sun, W. Ni, Z. Yang, X. Kou, L. Li and J. Wang, *Small*, 2008, **4**, 1287-1292.
68. H.-S. Park, A. Agarwal, N. A. Kotov and O. D. Lavrentovich, *Langmuir*, 2008, **24**, 13833-13837.
69. A. Indrasekara, R. C. Wadams and L. Fabris, *Part. Part. Syst. Charact.*, 2014, **31**, 819-838.